Fluctuating hydrodynamics for multiscale modeling and simulation: Energy and heat transfer in molecular fluids

Cite as: J. Chem. Phys. **137**, 044117 (2012); https://doi.org/10.1063/1.4738763
Submitted: 05 April 2012 • Accepted: 09 July 2012 • Published Online: 30 July 2012

Barry Z. Shang, Nikolaos K. Voulgarakis and Jhih-Wei Chu

Fluctuating hydrodynamics for multiscale modeling and simulation: Energy and heat transfer in molecular fluids

Barry Z. Shang, Nikolaos K. Voulgarakis, and Jhih-Wei Chu[a)]
Department of Chemical and Biomolecular Engineering, University of California Berkeley, Berkeley, California 94720, USA

(Received 5 April 2012; accepted 9 July 2012; published online 30 July 2012)

This work illustrates that fluctuating hydrodynamics (FHD) simulations can be used to capture the thermodynamic and hydrodynamic responses of molecular fluids at the nanoscale, including those associated with energy and heat transfer. Using all-atom molecular dynamics (MD) trajectories as the reference data, the atomistic coordinates of each snapshot are mapped onto mass, momentum, and energy density fields on Eulerian grids to generate a corresponding field trajectory. The molecular length-scale associated with finite molecule size is explicitly imposed during this coarse-graining by requiring that the variances of density fields scale inversely with the grid volume. From the fluctuations of field variables, the response functions and transport coefficients encoded in the all-atom MD trajectory are computed. By using the extracted fluid properties in FHD simulations, we show that the fluctuations and relaxation of hydrodynamic fields quantitatively match with those observed in the reference all-atom MD trajectory, hence establishing compatibility between the atomistic and field representations. We also show that inclusion of energy transfer in the FHD equations can more accurately capture the thermodynamic and hydrodynamic responses of molecular fluids. The results indicate that the proposed MD-to-FHD mapping with explicit consideration of finite molecule size provides a robust framework for coarse-graining the solution phase of complex molecular systems.
 [http://dx.doi.org/10.1063/1.4738763]

I. INTRODUCTION

Hydrodynamic fluctuations are important forces in affecting molecular transport at the nanometer to micrometer scales.[1] Self-assembly,[2] mixing,[3,4] capillary dynamics,[5–7] and molecular motor actions[8] are only several examples that are of fundamental as well as technological importance.[9] A key character about situating at a small length-scale that is absent at the macroscopic-scale counterpart is the significant influence of thermal energy. To capture hydrodynamics and thermal fluctuations under the same footing, a powerful theoretical framework is fluctuating hydrodynamics (FHD).[1,10,11] The FHD equations are stochastic partial differential equations that introduce stochastic fluxes into the conservation equations of momentum and energy transport to represent thermal noise. The magnitude of fluctuations depends on the grid size used to spatially discretize the system.[1,11] In the limit of large ($>\mu m^3$) volumes of grid cells, the deterministic conservation equations are recovered. In addition to solving the FHD equations directly in the Eulerian frame, the FHD equations have also been casted into different forms for developing mesoscale simulation methods such as fluctuating Lattice-Boltzmann[12] and smoothed dissipative particle dynamics.[13]

The explicit incorporation of thermal fluctuations into the conservation laws of continuum mechanics makes FHD an ideal framework for mesoscopic simulation. Indeed, some examples where FHD simulations have been applied include the modeling of Rayleigh-Taylor instability,[3] diffusive mixing of miscible fluids,[4] breakup of nanojets,[5] capillary wave phenomena,[6,7] droplet spreading,[14] and dynamics of nanoparticles[15–17] and polymers.[18,19] Numerical techniques for simulating the FHD equations are also being developed[20–25] and assessed.[21,26] However, the potential of using FHD as a framework to coarse-grain (CG) atomistic systems has not been much exploited. A key issue is whether consistency between FHD and all-atom molecular dynamics (MD) can be established. Specific concerns include whether a small length-scale (0.5–1 nm) of discretization is physically appropriate for solving the FHD equations in order to match with the all-atom MD model and how to bridge the observables of FHD and MD simulations to establish consistency in thermodynamic and hydrodynamic responses at different scales. These questions must be addressed before FHD can be applied as a framework for CG modeling of molecular fluids at the nanoscale.

To extend the accessible length- and time-scales of molecular simulation, an obvious strategy is reducing the degrees of freedom in the model by coarse-graining.[27] Since the solvent part often constitutes the majority of computational cost in molecular simulation, especially for all-atom MD, proper coarse-graining of the solvent is critical for successful modeling and simulation at the mesoscopic scale. Ideally, a coarse-graining method should be simple and be able to retain the essential physics for predicting the behaviors of the system of interest. In the category of explicit-solvent modeling, the most common approach is grouping one or more solvent molecules together into a bead.[28–31] An immediate difficulty of such particle-to-particle coarse-graining is that it is

a)Author to whom correspondence should be addressed. Electronic mail: jwchu@berkeley.edu.

very difficult to control bulk and interfacial properties separately through the pair potentials between particles.[31,32] Using a field-theoretic framework to coarse-grain the solution phase, on the other hand, not only removes the computational cost of tracking the positions and neighbor list of the solvent beads but also allows interfacial properties to be tuned separately from the bulk equation of state.[7] Furthermore, for particle-based coarse-graining, connection to experimental transport coefficients such as viscosity is only implicit through the interaction potentials and friction coefficients in the equations of motion.[29,31,33] In field-theoretic coarse-graining using the FHD simulations, on the other hand, the system dynamics are explicitly controlled by the equations of state and transport coefficients of the fluid, making the connection to experimental dynamics explicit.[1,10,11]

Utilizing FHD as a framework for multiscale modeling is also advantageous in connecting the CG model with the atomistic-scale simulation. It has been shown that an all-atom MD trajectory can be mapped onto hydrodynamic fields of mass and momentum to establish common observables between MD and FHD simulations.[25] By matching the statistics of common observables, the FHD model can be parameterized to be consistent with the finer resolution all-atom model.[7,25,34,35] A key finding is that for such consistency to hold at the sub-nanometer length-scale, the finite sizes of atoms or molecules need to be explicitly considered in mapping the atomistic configurations and velocities onto field variables.[7,25,34,35] This consideration is necessary to ensure that thermodynamic and hydrodynamic responses of the fluid are preserved at the coarser scale. In the regard of performing FHD simulations, it has been established that a staggered finite volume scheme allows the FHD equations to be solved with high accuracy in satisfying the fluctuation-dissipation theorem at 300 K even if the grid size is as small as 5 Å.[25] The combination of mapping all-atom MD onto fields and constructing a corresponding FHD model has been applied to investigate (1) the viscoelastic response of molecular fluids at nanoscales[34,35] and (2) the interfacial properties that enable a fluid to phase separate and form interfaces,[7] but not yet to the responses of energy and heat transfer.

Therefore, this work aims to establish the applicability of FHD for coarse-graining the transport of energy via thermal fluctuations in all-atom MD simulations by generalizing the framework developed in Ref. 25. In particular, we couple the stochastic energy balance[1] with the equations of mass and momentum conservation according to FHD and identify the proper molecular length-scales for coarse-graining all-atom MD onto the FHD model to capture the behaviors of energy and heat transfer.

In short, the atomistic coordinates, velocities, and internal energies calculated in MD simulations are mapped onto hydrodynamic variables on grid cells of nanometer scale. The finite size of an atom or molecule is explicitly considered during mapping, and is identified based on the criterion that density fluctuations within a grid cell should scale inversely with grid cell volume.[11,25] We illustrate that the fluid properties of argon and water extracted from this MD-to-FHD mapping are in quantitative agreement with the values determined from conventional methods that are mapping-free. Therefore, the results of this work establish that even at the sub-nanometer length-scale of grid cells, FHD can capture the thermodynamic and hydrodynamic responses of all-atom MD, establishing the applicability of FHD as a framework of multiscale modeling for systems that involve energy and heat transfer (EHT) of molecular fluids. Furthermore, we show that including EHT in FHD equations more accurately captures the hydrodynamic responses encoded in all-atom MD simulations. We also investigate the effects of the nonlinear terms in FHD equations on the thermodynamic and hydrodynamic responses of molecular fluids.

The rest of the paper is organized as follows. In Sec. II, we provide the background on the FHD equations with EHT. In Sec. III, we describe the methods used to calculate fluid properties from the statistics of field variables. In Sec. IV, we describe the mapping procedure to convert atomistic coordinates into hydrodynamic fields and the calculations of fluid properties from the field representation of an all-atom MD trajectory. In Sec. V, we simulate the FHD model, using parameters obtained from MD, and demonstrate that hydrodynamic fluctuations and relaxation in the FHD model are consistent with those of MD. In Sec. VI, we summarize the results of this work.

II. FLUCTUATING HYDRODYNAMICS WITH ENERGY AND HEAT TRANSFER

A. Governing equations

The equations of FHD incorporate thermal fluctuations into fluid flow by modeling the time evolution of mass, momentum, and energy density fields via Langevin-type dynamics.[1,10,11,21] The governing equations for mass, momentum, and energy transfer are

$$\frac{\partial}{\partial t}\rho = -\nabla\cdot(\rho\mathbf{v}), \tag{1}$$

$$\frac{\partial}{\partial t}\rho\mathbf{v} = -\nabla\cdot(\rho\mathbf{v}\mathbf{v}) - \nabla\cdot(\mathbf{P}) - \nabla\cdot(\mathbf{\Pi}+\boldsymbol{\delta\Pi}), \tag{2}$$

$$\frac{\partial}{\partial t}\rho e = -\nabla\cdot(\rho e\mathbf{v}) - \nabla\cdot(\mathbf{P}\cdot\mathbf{v}) - \nabla\cdot(\mathbf{\Pi}+\boldsymbol{\delta\Pi})\cdot\mathbf{v} - \nabla\cdot(\mathbf{q}+\boldsymbol{\delta q}). \tag{3}$$

The field variables include the mass density ρ, momentum density $\rho\mathbf{v}$, total energy density e, and streaming velocity $\mathbf{v}$. The reversible (pressure), dissipative and fluctuating stress tensors are $\mathbf{R}$, $\mathbf{\Pi}$, and $\boldsymbol{\delta\Pi}$, respectively. For homogeneous fluids considered in this work, the pressure tensor is isotropic, $\mathbf{R} = -p\mathbf{I}$, where p is the thermodynamic pressure. The dissipative and fluctuating heat fluxes are $\mathbf{q}$ and $\boldsymbol{\delta q}$, respectively. The dissipative stress is assumed to be Newtonian

$$\mathbf{\Pi} = -\mu\left(\nabla\mathbf{v} + \nabla\mathbf{v}^T\right) - \left(\eta - \frac{2}{3}\mu\right)\nabla\cdot\mathbf{v}, \tag{4}$$

where μ is the shear viscosity and η is the bulk viscosity. The dissipative heat flux is modeled by Fourier's Law to represent conductive heat transfer with thermal conductivity, λ,

$$\mathbf{q} = -\lambda\nabla T. \tag{5}$$

The fluctuating forces in momentum and energy transfer are described as Gaussian white noise with zero mean and covariance according to the fluctuation–dissipation theorem,[1,10,11]

$$\langle \delta\Pi_{ij}(\mathbf{r},t)\delta\Pi_{kl}(\mathbf{r}',t')\rangle = 2k_BT_0\Big[\mu(\delta_{il}\delta_{jk}+\delta_{ik}\delta_{jl}) + \left(\eta-\frac{2}{3}\mu\right)\delta_{ij}\delta_{kl}\Big]\delta(\mathbf{r}-\mathbf{r}')\delta(t-t'), \quad (6)$$

$$\langle \delta q_i(\mathbf{r},t)\,\delta q_j(\mathbf{r}',t')\rangle = 2\lambda k_B T_0^2\delta_{ij}\delta(\mathbf{r}-\mathbf{r}')\delta(t-t'). \quad (7)$$

The magnitude of the stochastic fluxes is governed by the equilibrium temperature T_0. The dissipative and fluctuating forces represent the effective contribution from the microscopic degrees of freedom that have been coarse-grained away.

In this work, we consider liquids with fluctuations close to equilibrium and employ a linear equation of state,[25]

$$P(\rho,T) = \frac{1}{\rho_0\kappa_T}\rho + \frac{\alpha_P}{\kappa_T}T. \quad (8)$$

This approximation will be verified in Sec. V, since the fluctuations calculated from all-atom MD are essentially Gaussian. To close the system of equations, the energy balance is now written in terms of the temperature T as in Ref. 1:

$$\frac{\partial}{\partial t}\rho c_V T = -\nabla\cdot(\rho c_V T\mathbf{v}) - \frac{T\alpha_P}{\kappa_T}\nabla\cdot\mathbf{v} - \nabla\cdot(\mathbf{q}+\delta\mathbf{q}). \quad (9)$$

The constant volume specific heat is c_V, the thermal expansivity is α_P, and the isothermal compressibility is κ_T. The temperature equation follows from the differential relation between the specific internal energy, temperature, and mass density.

Therefore, this work generalizes the model presented in Ref. 25 by incorporating EHT into the FHD equations. The FHD model with EHT is a more complete CG representation for atomistic systems because energy is constantly being exchanged at nanometer scales due to spontaneous fluctuations, even in isothermal systems at equilibrium. Therefore, the temperature degree of freedom is explicitly considered here. The additional parameters introduced by incorporating EHT into the FHD equations are the specific heat c_V, thermal expansivity α_P, and thermal conductivity λ.

B. Linearized FHD model

In this section, the linearized FHD equations are introduced,[1,10,11,36,37] which will be later used to assist in parameterizing the full nonlinear FHD model from MD simulations. The linear equations allow analytic expressions to be derived that relate response functions and transport coefficients to the fluctuations and time correlation functions of the hydrodynamic field variables. Therefore, the fluid properties of an atomistic model can be estimated by fitting the MD data to these analytical expressions as the starting point; the details of model parameterization will be discussed in Sec. III. The linearized FHD equations are

$$\frac{\partial}{\partial t}\delta\rho = -\rho_0\nabla\cdot\boldsymbol{\delta}\mathbf{v}, \quad (10)$$

$$\rho_0\frac{\partial}{\partial t}\boldsymbol{\delta}\mathbf{v} = -\nabla\delta P + \mu\nabla^2\boldsymbol{\delta}\mathbf{v} + \left(\eta+\frac{1}{3}\mu\right)\nabla(\nabla\cdot\boldsymbol{\delta}\mathbf{v}) - \nabla\cdot\boldsymbol{\delta}\boldsymbol{\Pi}, \quad (11)$$

$$\rho_0 c_V\frac{\partial}{\partial t}\delta T = -\frac{T_0\alpha_P}{\kappa_T}\nabla\cdot\boldsymbol{\delta}\mathbf{v} + \lambda\nabla^2\delta T - \nabla\cdot\boldsymbol{\delta}\mathbf{q}. \quad (12)$$

The fluctuations of field variables are $\delta\phi = \phi - \phi_0$, where $\phi = \{\rho, \mathbf{v}, T\}$, and ϕ_0 is the equilibrium average. The fluctuation of the local pressure δP is related to the density and temperature fluctuations by[1,36]

$$\delta P = \frac{1}{\rho_0\kappa_T}\delta\rho + \frac{\alpha_P}{\kappa_T}\delta T. \quad (13)$$

III. THE CALCULATION OF FLUID PROPERTIES

To obtain parameters for the FHD equations, the response functions (κ_T, c_V, α_P) and transport coefficients (μ, η, λ) are calculated from an all-atom MD trajectory by mapping atomistic coordinates onto density fields with explicit consideration of the finite sizes of atoms or molecules. The values of these fluid properties are compared with those obtained via mapping-free methods to assess the accuracy of the mapping procedure. Using the calculated fluid properties in an FHD simulation, we show later in Sec. IV that the resulting fluctuations and relaxation of field variables quantitatively match with those observed in the reference all-atom MD trajectory, thereby establishing compatibility between FHD and MD models.

A. Response functions

1. With the MD-to-FHD mapping

To map atomistic coordinates onto density fields, the MD simulation box is discretized into cubic grids, and the atomistic coordinates in each snapshot in the MD trajectory are then used to calculate the mass and internal energy density of each grid. Details of this mapping will be described later. The all-atom MD trajectory is thus transformed into a field trajectory. Since each grid cell can be viewed as an open system that contains a grand canonical ensemble of microstates, response functions can be determined from the density fluctuations within each grid.[38,39] The isothermal compressibility is

$$\kappa_T = \frac{\langle(\delta\rho)^2\rangle_{\mu VT}V_G}{\rho^2 k_B T}, \quad (14)$$

the specific heat is

$$c_V = \frac{V_G}{\rho k_B T^2}\left(\langle(\delta u)^2\rangle_{\mu VT} - \frac{\langle\delta u\delta\rho\rangle_{\mu VT}}{\langle(\delta\rho)^2\rangle_{\mu VT}}\right), \quad (15)$$

and the thermal expansivity is

$$\alpha_P = \frac{\kappa_T}{T}(P+\varepsilon) - \frac{\langle \delta\varepsilon\delta\rho\rangle_{\mu VT}\, V_G}{\rho k_B T^2}. \tag{16}$$

In the above equations, u is the internal energy density, P is the pressure, and ε is the potential energy density. Thermal averages are taken over the grand canonical ensemble μVT distribution. Equations (14)–(16) also follow from the Gaussian stationary distribution satisfied by the linearized FHD equations.[1,37,40]

2. Without the MD-to-FHD mapping

To assess the results obtained via mapping to grid cells, response functions are also computed using an alternative method that does not involve mapping. In particular, all-atom MD simulations of a molecular system are performed under both *NVT* and *NPT* conditions, and appropriate formulas[38] are used to determine the response functions. In particular, the compressibility can be calculated as

$$\kappa_T = \frac{\langle (\delta V)^2\rangle_{NPT}}{V k_B T}, \tag{17}$$

the specific heat can be calculated as

$$c_V = \frac{\langle (\delta U)^2\rangle_{NVT}}{\rho V k_B T^2}, \tag{18}$$

and the thermal expansivity can be calculated as

$$\alpha_P = \frac{\langle \delta V \delta (U+PV)\rangle_{NPT}}{V k_B T^2}. \tag{19}$$

In the above equations, V is the volume of the MD simulation box and U is the total internal energy. Response functions calculated using Eqs. (14)–(16) will be compared with those calculated from Eqs. (17)–(19) to assess the accuracy of the mapping scheme.

B. Transport coefficients

1. With the MD-to-FHD mapping

Transport coefficients are calculated from all-atom MD using the mapping scheme followed by computing the time correlation functions of density and velocity fields in Fourier space. The results are then fit to analytical expressions derived from the linearized FHD equations. The density time correlation function from linearized FHD is[1,11,36]

$$\begin{aligned} C_\rho &= \frac{\langle \rho(-k,0)\rho(k,t)\rangle}{\langle |\rho(k,0)|^2\rangle} \\ &= \frac{\gamma-1}{\gamma}\exp\left(-D_T k^2 t\right) + \frac{1}{\gamma}\cos(c_S k t)\exp(-\Gamma k^2 t). \end{aligned} \tag{20}$$

The specific heat ratio is $\gamma = c_P/c_V$, the thermal diffusivity is $D_T = \lambda/\rho c_P$, the sound attenuation coefficient is $\Gamma = 1/2\,(D_V + (\gamma-1)\,D_T)$, and the sound speed is $c_S = (\gamma/\rho\kappa_T)^{1/2}$. The longitudinal kinematic viscosity is $D_V = (4\mu/3+\eta)/\rho$, and k is the wave number.

For transverse velocity, the correlation function is[11]

$$C_{v,t} = \frac{\langle v_t(-k,0)v_t(k,t)\rangle}{\langle |v_t(k,0)|^2\rangle} = \exp(-\nu k^2 t), \tag{21}$$

where $\nu = \mu/\rho$ is the kinematic shear viscosity, while for longitudinal velocity,[11]

$$C_{v,l} = \frac{\langle v_l(-k,0)v_l(k,t)\rangle}{\langle |v_l(k,0)|^2\rangle} = \cos(c_S k t)\exp(-\Gamma k^2 t), \tag{22}$$

which is valid for small k. In our analysis, we choose the wave vector to point in the z-direction, i.e., $\mathbf{k} = (0, 0, k)$, so $v_t = v_{x,y}$ and $v_l = v_z$.

2. Without the MD-to-FHD mapping

As an independent check, transport coefficients can also be determined from all-atom MD data without mapping to grid cells by using the Green-Kubo relations.[11,41,42] The shear viscosity is related to the relaxation of the microscopic pressure as

$$\mu = \frac{V}{k_B T}\int_0^\infty \left\langle \tilde{P}_{\alpha\beta}(0)\,\tilde{P}_{\alpha\beta}(t)\right\rangle dt. \tag{23}$$

The bulk viscosity is

$$\eta = \frac{V}{k_B T}\int_0^\infty \left\langle \delta\tilde{P}(0)\,\delta\tilde{P}(t)\right\rangle dt, \tag{24}$$

where $\delta\tilde{P}(t) = (1/3)\sum_\alpha \tilde{P}_{\alpha\alpha}(t) - \left\langle \tilde{P}_{\alpha\alpha}\right\rangle$, and the thermal conductivity is

$$\lambda = \frac{V}{k_B T^2}\int_0^\infty \left\langle \tilde{J}_\alpha(0)\,\tilde{J}_\alpha(t)\right\rangle dt. \tag{25}$$

In the above, $\tilde{P}_{\alpha\beta}$ are the components of the microscopic pressure[11,38,41] and $\tilde{J}_\alpha$ are the components of the microscopic heat flux.[11,41] Transport coefficients calculated using Eqs. (20)–(22) will be compared with those calculated from Eqs. (23)–(25) to assess the accuracy of the mapping scheme.

To establish consistency between FHD and MD models, we next describe the mapping of atomistic coordinates from MD simulation onto density fields, taking into account finite atomistic sizes, and analyze the field trajectory obtained from MD to calculate fluid properties, which are used later as input into FHD simulations.

IV. MAPPING AN ALL-ATOM MD TRAJECTORY ONTO SNAPSHOTS OF FIELD CONFIGURATIONS

In this section, we describe the details of all-atom MD simulations and our proposed mapping scheme. In particular, we show that the finite size of an atom or molecule needs to be explicitly considered to ensure that the magnitude of density fluctuations is inversely proportional to the volume of grid cells; see also Eqs. (14)–(16). Liquid argon and water are employed as illustrative examples.

A. Simulation details

For both argon and water, all-atom MD simulations were performed in the *NVT* ensemble using a Nosé-Hoover thermostat[43] in a 60 Å cubic box with periodic boundary conditions for 10 ns. Lennard-Jones (LJ) interactions were smoothly switched off from 10 Å to 12 Å. The time step is 2 fs, the neighbor list was updated every 10 integration steps, and a snapshot was saved every 0.1 ps. For argon, the LJ parameters are $\varepsilon = 0.238$ kcal/mol, $\sigma = 3.405$ Å,[44] and the atomic mass is 39.948 amu. Simulation conditions for argon were $T = 86.5$ K, and $\rho = 0.844$ amu/Å^3. For water, the TIP3P potential was used with particle-mesh Ewald[45] to compute electrostatic interactions and the SHAKE algorithm[46] to constrain bond lengths. Simulation conditions for water were $T = 300$ K and $\rho = 0.603$ amu/Å^3. To compute response functions from fluctuation formulas, *NPT* simulations were also performed via the Langevin piston method.[47] To compute time correlation functions, simulations were performed under *NVE* conditions with a box size of 60 × 60 × 240 Å and a simulation time of 50 ns.

To map atomistic positions and velocities onto mass, momentum, and energy density fields, the simulation box was first discretized into an array of cubic grids varying in size from 5 Å to 20 Å. Each argon atom or water molecule was also discretized as a space-filling cube. For each grid, the total mass m, momentum $\mathbf{p}$, and internal energy U are calculated as

$$m = \sum_i \phi_i m_i, \tag{26}$$

$$\mathbf{p} = \sum_i \phi_i \mathbf{p}_i, \tag{27}$$

$$U = \sum_i \phi_i \left(U_{K,i} + U_{P,i}\right), \tag{28}$$

where the sum i runs over atoms (argon) or molecules (water). The volume fraction ϕ_i is the volume of an atom or molecule that overlaps with the grid divided by the total volume of the atom or molecule. The kinetic contribution to the potential energy is calculated as $U_{K,i} = (1/2)\sum_j m_j \left(\mathbf{v}_j - \mathbf{v}\right)^2$, where the sum j runs over the atoms of molecule i, and the streaming velocity in a grid is $\mathbf{v} = \mathbf{p}/m$. The potential energy $U_{P,i}$ includes Lennard-Jones and the real-space electrostatic interactions (for water). To determine errors introduced by neglecting the long-range contributions, the real-space contribution was gradually increased when computing the potential energy until the response functions became independent of the cutoff. We found that this convergence occurs at a cutoff around 42 Å. To determine the volume fraction inside a grid, each argon atom or water molecule is modeled as a cube with length d_{mol}. For water, the geometric center of the cube coincides with the molecule center of mass. Physically, this means the mass, momentum, and internal energy of an atom or molecule is spread uniformly over a cube with side length of d_{mol}.

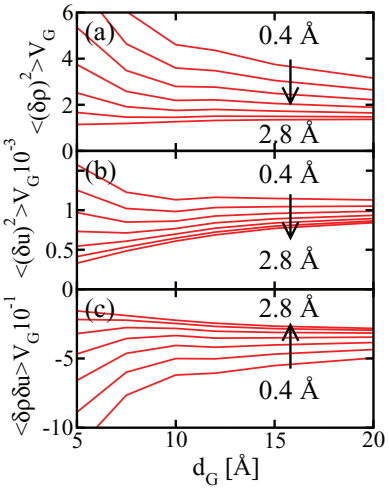

FIG. 1. Conversion of the snapshots in an all-atom MD simulation into a trajectory of field variables by the MD-to-FHD mapping with d_{mol} using different length-scales for coarse-graining the solvent molecules. Variances of the fluctuations of (a) mass density ρ and (b) internal energy density u of argon as a function of the length of cubic grid cells, d_G, and the molecular length-scale of coarse-graining, d_{mol}. (c) Covariance of ρ and u fluctuations. The volume of the grid cell is $V_G = d_G^3$. Lines are plotted for d_{mol} ranging from 0.4 Å to 2.8 Å with 0.4 Å increments. Units are ρ (amu/Å^3), u (amu Å^2/ps^2), V_G(Å^3), and d_{mol}(Å).

B. Fluid properties from MD

After mapping with d_{mol}, fluctuations of mass and energy density fields in each cell volume are used to calculate the response functions encoded in an all-atom MD trajectory. For a grid size in the nanometer regime, the magnitude of fluctuations also depends on the molecular length scale d_{mol}.[25] A criterion based on statistical mechanics for determining d_{mol} is that the variances of density fluctuations within a grid should scale inversely with grid cell volume. The fluctuations of mass and internal energy densities mapped from all-atom MD trajectories are plotted as a function of cubic grid length d_G and molecule size d_{mol} for argon and water in Figs. 1 and 2, respectively. For argon, the optimal d_{mol} based on the criterion of size consistent scaling of variances is 2.4 Å for mass density and 0.4 Å for energy density. For water, the optimal d_{mol} is 2.2 Å for mass density and 1.8 Å for energy density. For the covariance of mass and energy density, the optimal d_{mol} is 1.6 Å for argon and 2.0 Å for water. In general, density fluctuations gradually become overestimated with decreasing d_{mol}, as the molecule mass is over-concentrated in a small volume. On the other hand, density fluctuations gradually become underestimated with the increasing d_{mol}, since volumes of different molecules overlap and cause artificial correlation. For larger grid sizes, the effects of d_{mol} become less significant, as the open system of a given grid cell is closer to the thermodynamic limit. The response functions are computed from the covariances via Eqs. (14)–(16) using the optimal values of d_{mol} and a grid size of 10 Å, the same grid size that is used in FHD simulations. In Table I, the response functions obtained via mapping to grids are listed, which agree well with results obtained from *NVT* and *NPT* simulations, affirming the self-consistency of mapping with d_{mol}. The inverse scaling of variances with grid volume down to 5 Å-sized grids, observed in

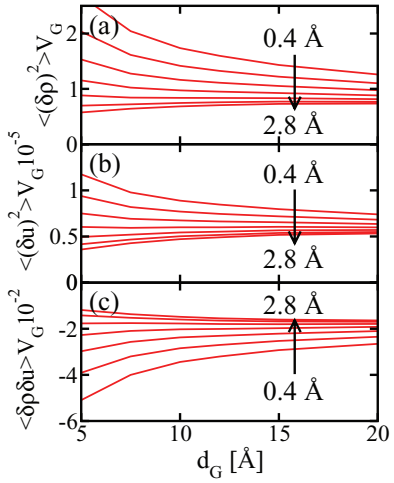

FIG. 2. Conversion of the snapshots in an all-atom MD simulation into a trajectory of field variables by the MD-to-FHD mapping with d_{mol} using different length-scales for coarse-graining the solvent molecules. Variances of the fluctuations of (a) mass density ρ and (b) internal energy density u of water as a function of the length of cubic grid cells, d_G, and the molecular length-scale of coarse-graining, d_{mol}. (c) Covariance of ρ and u fluctuations. The volume of the grid cell is $V_G = d_G^3$. Lines are plotted for d_{mol} ranging from 0.4 Å to 2.8 Å with 0.4 Å increments. Units are ρ(amu/Å^3), u(amu Å^2/ps^2), V_G(Å^3), and d_{mol}(Å).

Figs. 1 and 2, also underscores that the thermodynamic limit is satisfied even at sub-nanometer length scales, ensuring that an FHD model employing nanometer spatial discretization can be valid.

The observation that the thermodynamic limit holds even at molecular length scales has also been supported by calculations of local stress tensor fluctuations in LJ liquids,[48] which exhibit an inverse scaling with volume down to length-scales on the order of the size of the atom. These calculations also show that spatial covariances of the local stress tensor become uncorrelated at distances less than two LJ diameters, confirming the delta function assumption made in fluctuating stress in Eq. (6). In these studies, the temporal correlations also appear to decay rapidly, justifying the use of white noise in the FHD equations.

TABLE I. Response functions of liquid argon and water calculated by mapping with d_{mol} and without mapping. Values calculated with the MD-to-FHD mapping were calculated using Eqs. (14)–(16), while values without the MD-to-FHD mapping were calculated using Eqs. (17)–(19). The isothermal compressibility is κ_T (atm^{-1}), the constant volume specific heat capacity is c_V (cal/mol K), and the thermal expansivity is α_P (K^{-1}). Standard errors are determined from results using three independent MD simulations of 1 ns each.

Argon	With the MD-to-FHD mapping	Without the MD-to-FHD mapping
$\kappa_T \times 10^{-4}$	1.7 ± 0.2	2.1 ± 0.2
c_V	2.5 ± 0.5	2.3 ± 0.1
$\alpha_P \times 10^{-3}$	3.6 ± 0.2	3.6 ± 0.1
Water		
$\kappa_T \times 10^{-5}$	5.3 ± 0.1	5.6 ± 0.6
c_V	16.7 ± 0.2	16.8 ± 0.4
$\alpha_P \times 10^{-4}$	7.4 ± 0.2	7.5 ± 0.5

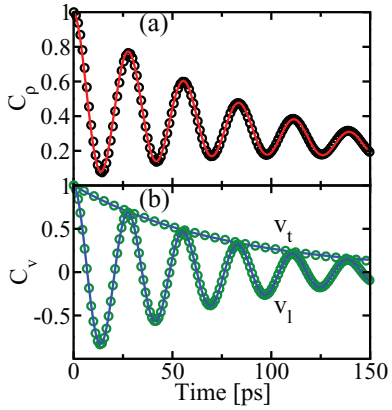

FIG. 3. Time correlation functions of (a) mass density and (b) transverse v_t and longitudinal v_l velocity of argon at 86.5 K and 66 atm. The wave vector is $\mathbf{k} = (0, 0, k)$, where $k = 2\pi/240$ Å^{-1}. All-atom MD results are shown as circles, while the best-fit curves of Eqs. (20)–(22) are shown as solid lines.

To determine transport coefficients, the density and velocity time correlation functions were computed from the mapped coordinates and fitted to Eqs. (20)–(22), using both transport coefficients and response functions as adjustable parameters. The correlation functions and the resulting fit are shown for argon in Fig. 3 and for water in Fig. 4. The best-fit transport coefficients listed in Table II agree well with the values obtained from independent Green-Kubo calculations. In addition, the best-fit response functions obtained through mapping with d_{mol} also agree well with the values listed in Table I (results not shown). These results underscore the importance of accounting for finite molecule size d_{mol} upon coarse-graining atomistic coordinates to density fields. This procedure ensures that the values of fluid properties are preserved upon mapping atomistic positions, velocities, and interaction energies onto field variables.

We note that in prior work,[49–51] others have computed mass density and velocity time correlation functions and fit these results to analytical predictions from linearized hydrodynamics to obtain fluid properties. The distinction of this

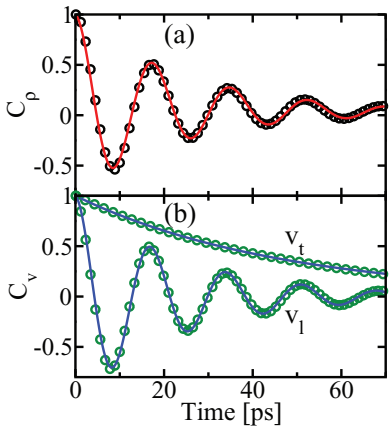

FIG. 4. Time correlation functions of (a) mass density and (b) transverse v_t and longitudinal v_l velocity of liquid water at 300 K and 1 atm. The wave vector is $\mathbf{k} = (0, 0, k)$, where $k = 2\pi/240$ Å^{-1}. All-atom MD results are shown as circles, while the best-fit curves of Eqs. (20)–(22) are shown as solid lines.

TABLE II. Transport coefficients of liquid argon and water calculated by mapping with d_{mol} and without mapping. Values calculated with the MD-to-FHD mapping were obtained via best-fitting to Eqs. (20)–(22), while values without the MD-to-FHD mapping were obtained via the Green-Kubo relations in Eqs. (23)–(25). The shear viscosity is μ (cP), the bulk viscosity is η (cP), and the thermal conductivity is λ (W/mK). Standard errors are determined from results using three independent MD simulations of 50 ns each (mapping) and 10 ns each (without mapping).

Argon	With the MD-to-FHD mapping	Without the MD-to-FHD mapping
μ	0.27 ± 0.02	0.28 ± 0.02
η	0.09 ± 0.02	0.10 ± 0.01
λ	0.13 ± 0.03	0.12 ± 0.01
Water		
μ	0.31 ± 0.01	0.32 ± 0.01
η	0.77 ± 0.04	0.77 ± 0.05
λ	1.04 ± 0.03	0.99 ± 0.03

work from such analyses is that our MD-to-FHD mapping concerns the coarse-graining from the atomistic phase space onto the density fields on grid cells. The earlier works, on the other hand, computed the time correlation functions by off-lattice Fourier transform and were primarily interested in assessing the dependence of fluid properties on wave number. As a result, for modeling complex systems with spatial heterogeneity, our coarse-graining method can provide the required generality.

V. SIMULATION WITH FHD EQUATIONS

In this section, we present results of FHD simulations with energy and heat transfer using the response functions and transport coefficients of argon and water calculated from the MD-to-FHD mapping with d_{mol}. We illustrate that the density, velocity, and temperature fluctuations observed in FHD and MD simulations quantitatively agree with each other. We also show that density and velocity time correlation functions between the FHD and MD simulations are matched. These results demonstrate that the FHD model accurately describes the emergent hydrodynamic fluctuations of molecular fluids and is a promising tool for coarse-graining the solvent in multiscale simulations.

A. Simulation details

FHD simulations were performed for argon and water in a 60 Å cubic box replicated periodically and discretized by 10 Å cubic grids. The total simulation time was 10 ns, the time step was 5 fs, and a snapshot was saved every 0.1 ps. Simulation conditions were, for argon, $T = 86.5$ K and $\rho = 0.844$ amu/Å^3, and for water, $T = 300$ K and $\rho = 0.603$ amu/Å^3. These conditions are identical to those used in all-atom MD simulations. To compute time correlation functions, simulations were performed using a box size of $60 \times 60 \times 240$ Å and a simulation time of 50 ns. The FHD equations are solved using a staggered finite volume scheme in space and second-order Runge-Kutta integration in time.[25] Details for the random number generation for the stochastic fluxes can be found in Ref. 34. The FHD input parameters are the response functions (κ_T,c_V,α_P) and transport coefficients (μ,η,λ), which were determined previously from the MD-to-FHD mapping.

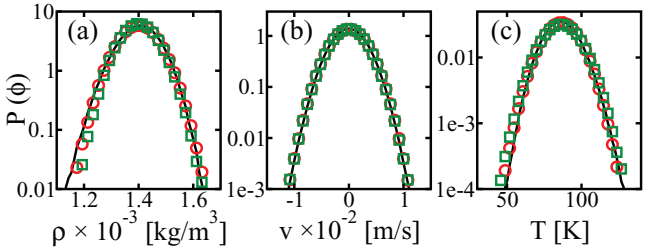

FIG. 5. Probability distribution functions of (a) mass density, (b) streaming velocity, and (c) temperature of liquid argon at 86.5 K and 66 atm. The streaming velocity is defined in Sec. IV, and the temperature is defined in Eq. (29). Results of the all-atom MD simulation are shown as black curves. Results of the linear and nonlinear FHD simulations are shown as red circles and green squares, respectively. $\phi = \rho$, v, or T.

B. FHD-MD consistency in the statistics of fluctuations

We compare the fluctuations of mass density, streaming velocity, and temperature within a grid cell observed in MD and FHD simulations. Before doing so, we first establish the connection of the fluctuating temperature to molecular mechanical variables. From thermodynamic fluctuation theory,[11,40,52] the fluctuating temperature can be estimated by expanding the internal energy density fluctuation to linear order in temperature and mass density

$$\delta u = \left(\frac{\partial u}{\partial T}\right)_\rho \delta T + \left(\frac{\partial u}{\partial \rho}\right)_T \delta\rho. \tag{29}$$

In the above equation, $(\partial u/\partial T)_\rho = \rho c_V$, where c_V is found from Eq. (15). The temperature and mass density fluctuations are uncorrelated,[11,40,52] which implies[52]

$$\left(\frac{\partial u}{\partial \rho}\right)_T = \frac{\langle \delta u \delta\rho \rangle}{\langle (\delta\rho)^2 \rangle}. \tag{30}$$

Equations (15), (29), and (30) allow the temperature within each grid to be determined from the mass and internal energy density fluctuations in the MD simulation. After mapping with d_{mol}, the fluctuating temperature fields in each grid cell represent the part of the internal energy density fluctuation that is uncorrelated with mass density.

In Figs. 5 and 6, the probability distributions for mass density, streaming velocity, and temperature from MD and FHD simulations are compared for argon and water, respectively. The results from linear and nonlinear FHD simulations are both shown to illustrate the effects of nonlinear advection on these fluctuations. As expected, solving the linearized FHD equations with the response functions obtained from MD using the analytic formulas gives rise to statistics that quantitatively agree with those extracted from MD directly. This result illustrates that the FHD equations can be solved accurately with a nanometer-scale discretization. The presence of nonlinear advection appears to affect the equilibrium fluctuations only slightly. Therefore, under the conditions of MD simulation conducted in this work, advection does not

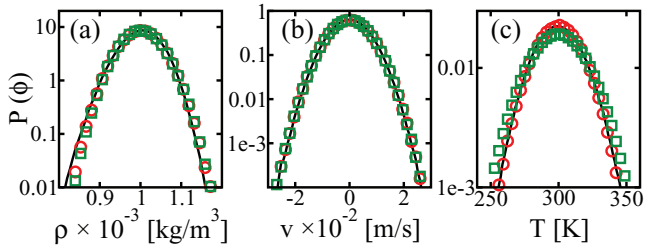

FIG. 6. Probability distribution functions of (a) mass density, (b) streaming velocity, and (c) temperature of liquid water at 300 K and 1 atm. The streaming velocity is defined in Sec. IV, and the temperature is defined in Eq. (29). Results of the all-atom MD simulation are shown as black curves. Results of the linear and nonlinear FHD simulations are shown as red circles and green squares, respectively. $\phi = \rho$, v, or T.

have an appreciable effect on the equilibrium distributions and hence the equation of state. The agreement between the atomistic and CG scales indicates that by mapping atomistic trajectories onto hydrodynamic fields with scaling consistency by optimizing d_{mol}, an FHD model can be developed to capture the thermodynamic responses of the molecular fluid.

C. FHD-MD consistency in time correlation functions

The time correlation functions obtained from the MD simulation and the linear and nonlinear FHD simulations are plotted in Fig. 7 for argon and in Fig. 8 for water. Since the response functions and transport coefficients used in FHD simulations are determined by analyzing the field representation of all-atom MD trajectories with linearized hydrodynamics, the correlation functions calculated from the linearized FHD simulations indeed match with those calculated from all-atom MD. Therefore, solving the FHD equations with nanometer-scale discretization also gives an accurate representation of the dynamics of molecular fluids. As seen in Figs. 7 and 8, the primary difference between the linear and nonlinear correlation functions for both argon and water is that the oscillation

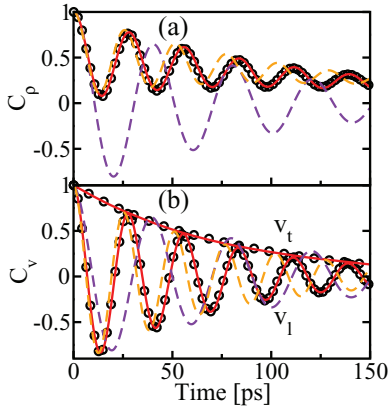

FIG. 7. Time correlation functions of (a) mass density and (b) transverse v_t and longitudinal v_l velocity of liquid argon at 86.5 K and 66 atm. The wave vector is $\mathbf{k} = (0, 0, k)$, where $k = 2\pi/240$ Å^{-1}. Results of the all-atom MD simulation are shown as black circles. Results of the linear and nonlinear FHD simulations with energy transfer are shown as solid red and dotted orange curves, respectively. The dotted purple curve shows the result of FHD simulations without energy transfer.

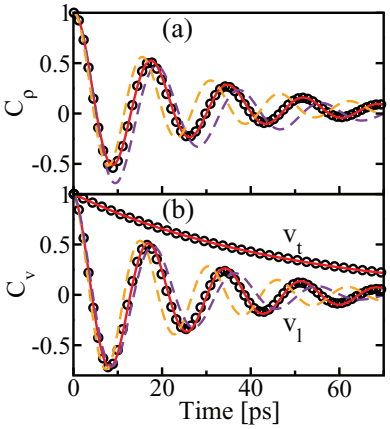

FIG. 8. Time correlation functions of (a) mass density and (b) transverse v_t and longitudinal v_l velocity of liquid water at 300 K and 1 atm. The wave vector is $\mathbf{k} = (0, 0, k)$, where $k = 2\pi/240$ Å^{-1}. Results of the all-atom MD simulation are shown as black circles. Results of the linear and nonlinear FHD simulations with energy transfer are shown as solid red and dotted orange curves, respectively. The dotted purple curve shows the result of FHD simulations without energy transfer.

period is about 10% less due to the additional flux from advection. Fitting the MD results to the linear correlation function thus slightly underestimates the fluid compressibility, and can be easily corrected by iteration through simulations using the nonlinear FHD model. Since this underestimation is within the statistical uncertainties of the MD results presented in Table I, satisfactory agreement between MD and nonlinear FHD simulations is achieved for both fluids even without iteration. With the MD-to-FHD mapping, the time scales in the all-atom and FHD models can be transparently compared and synchronized, which remains difficult in current particle-based CG models.[29,31,33]

In addition, Figs. 7 and 8 also show the time correlation functions obtained by solving the FHD equations without EHT. In this case, the effects of the advection term on the time correlation functions become unnoticeable, indicating that the primary contribution of nonlinearity lies in the advection of energy directly, rather than momentum through fluid flow. Clear deviation of the results using the simpler model without EHT from the all-atom MD results is observed. The difference is larger for argon due to its higher specific heat ratio (2.1 vs. 1.1 for water), which enhances the dissipative contribution from the thermal diffusivity, as suggested by Eq. (20). Therefore, to accurately capture the dynamics of a molecular fluid in a CG representation, it is important to include the energy transport equation to capture the coupling between mass and energy transfer. The results show that the FHD equations with energy transfer-–along with a self-consistent MD-to-FHD mapping—can be used to coarse-grain a molecular fluid to preserve both the thermodynamic and hydrodynamic responses.

VI. CONCLUSION

In this work, the FHD equations are shown to accurately capture the thermodynamic responses and hydrodynamic relaxation of molecular fluids, including those associated with energy and heat transfer. The results thus endorse FHD as a

promising framework to coarse-grain the liquid phase environment in complex molecular systems. An essential component in connecting MD and FHD is a mapping procedure that converts atomistic positions, masses, velocities, and interaction energies into density fields of mass, momentum, and energy on Eulerian grid cells. For nanometer grids, the finite size of an atom or molecule needs to be explicitly considered to ensure that the variances of density fluctuations scale inversely with grid volume, and that the density fluctuations are consistent with the response functions of the fluid. An important finding is that for different hydrodynamic variables, different molecule sizes are required in order to achieve the correct scaling of the fluctuations with grid size. Remarkably, the mass and energy density fluctuations obey this inverse scaling for grid sizes down to 5 Å, affirming the applicability of FHD modeling at the nanoscale. By using fluid properties extracted from all-atom MD simulations to simulate the FHD equations, the resulting fluctuations of mass density, streaming velocity, and temperature are shown to quantitatively agree with those observed in all-atom MD simulations. This result indicates that the FHD equations with energy and heat transfer can be solved accurately with nanometer-scale discretization. Furthermore, dynamical relaxations in FHD simulations also synchronize with those observed in all-atom MD simulations. Therefore, the proposed procedure of converting and matching common observables between MD and FHD simulations is capable of establishing thermodynamic and hydrodynamic compatibility between atomistic and hydrodynamic representations of a fluid. The results of this work indicate that FHD modeling can be used as an accurate and robust framework for coarse-graining the solution phase of complex molecular systems.

ACKNOWLEDGMENTS

We thank the University of California, Berkeley for financial support. B.Z.S. also acknowledges the National Science Foundation for financial support.

[1] J. O. d. Zarate and J. Sengers, *Hydrodynamic Fluctuations in Fluids and Fluid Mixtures* (Elsevier, New York, 2006).
[2] K. Lum, D. Chandler, and J. D. Weeks, J. Phys. Chem. B **103**, 4570 (1999).
[3] K. Kadau, C. Rosenblatt, J. L. Barber, T. C. Germann, Z. Huang, P. Carlès, and B. J. Alder, Proc. Natl. Acad. Sci. U.S.A. **104**, 7741 (2007).
[4] A. Donev, A. de la Fuente, J. B. Bell, and A. L. Garcia, Phys. Rev. Lett. **106**, 204501 (2011).
[5] M. Moseler and U. Landman, Science **289**, 1165 (2000).
[6] R. Delgado-Buscalioni, E. Chacon, and P. Tarazona, Phys. Rev. Lett. **101**, 106102 (2008).
[7] B. Z. Shang, N. K. Voulgarakis, and J. W. Chu, J. Chem. Phys. **135**, 044111 (2011).
[8] P. Hänggi and F. Marchesoni, Rev. Mod. Phys. **81**, 387 (2009).
[9] L. Bocquet and E. Charlaix, Chem. Soc. Rev. **39**, 1073 (2010).
[10] L. D. Landau and E. M. Lifshitz, *Fluid Mechanics* (Pergamon, New York, 1959).
[11] J. P. Hansen and I. R. McDonald, *Theory of Simple Liquids*, 3rd ed. (Academic, London, 2006).
[12] B. Dünweg, U. D. Schiller, and A. J. C. Ladd, Phys. Rev. E **76**, 036704 (2007).
[13] P. Español and M. Revenga, Phys. Rev. E **67**, 026705 (2003).
[14] B. Davidovitch, E. Moro, and H. A. Stone, Phys. Rev. Lett. **95**, 244505 (2005).
[15] N. Sharma and N. A. Patankar, J. Comput. Phys. **201**, 466 (2004).
[16] A. Donev, J. B. Bell, A. L. Garcia, and B. J. Alder, Multiscale Model Simul. **8**, 871 (2010).
[17] B. Uma, T. N. Swaminathan, R. Radhakrishnan, D. M. Eckmann, and P. S. Ayyaswamy, Phys. Fluids **23**, 073602 (2011).
[18] P. Ahlrichs and B. Dünweg, J. Chem. Phys. **111**, 8225 (1999).
[19] G. Giupponi, G. De Fabritiis, and P. V. Coveney, J. Chem. Phys. **126**, 154903 (2007).
[20] A. L. Garcia, M. Malek Mansour, G. Lie, and E. Clementi, J. Stat. Phys. **47**, 209 (1987).
[21] J. B. Bell, A. L. Garcia, and S. A. Williams, Phys. Rev. E **76**, 016708 (2007).
[22] G. De Fabritiis, M. Serrano, R. Delgado-Buscalioni, and P. V. Coveney, Phys. Rev. E **75**, 026307 (2007).
[23] R. Delgado-Buscalioni and G. De Fabritiis, Phys. Rev. E **76**, 036709 (2007).
[24] R. Delgado-Buscalioni and A. Dejoan, Phys. Rev. E **78**, 046708 (2008).
[25] N. K. Voulgarakis and J. W. Chu, J. Chem. Phys. **130**, 134111 (2009).
[26] A. Donev, E. Vanden-Eijnden, A. L. Garcia, and J. B. Bell, Commun. Appl. Math. Comput. Sci. **5**, 149 (2010).
[27] *Coarse-Graining of Condensed Phase and Biomolecular Systems*, edited by G. A. Voth (CRC, Boca Raton, FL, 2009).
[28] R. D. Groot and K. L. Rabone, Biophys. J. **81**, 725 (2001).
[29] S. J. Marrink, H. J. Risselada, S. Yefimov, D. P. Tieleman, A. H. de Vries, J. Phys. Chem. B **111**, 7812 (2007).
[30] W. G. Noid, J. W. Chu, G. S. Ayton, V. Krishna, S. Izvekov, G. A. Voth, A. Das, and H. C. Andersen, J. Chem. Phys. **128**, 244114 (2008).
[31] R. D. Groot and P. B. Warren, J. Chem. Phys. **107**, 4423 (1997).
[32] X. He, W. Shinoda, R. DeVane, and M. L. Klein, Mol. Phys. **108**, 2007 (2010).
[33] S. Izvekov and G. A. Voth, J. Chem. Phys. **125**, 151101 (2006).
[34] N. K. Voulgarakis, S. Satish, and J. W. Chu, J. Chem. Phys. **131**, 234115 (2009).
[35] N. K. Voulgarakis, S. Satish, and J. W. Chu, Mol. Simul. **36**, 552 (2010).
[36] B. J. Berne and R. Pecora, *Dynamic Light Scattering* (Wiley, New York, 1976).
[37] R. F. Fox and G. E. Uhlenbeck, Phys. Fluids **13**, 1893 (1970).
[38] M. P. Allen and D. J. Tildesley, *Computer Simulation of Liquids*. (Clarendon, Oxford, 1987).
[39] D. J. Adams, Mol. Phys. **29**, 307 (1975).
[40] J. M. Rubí and P. Mazur, Physica A **276**, 477 (2000).
[41] D. A. McQuarrie, *Statistical Mechanics* (University Science Books, Sausalito, CA, 2000).
[42] R. Zwanzig, Annu. Rev. Phys. Chem. **16**, 67 (1965).
[43] W. G. Hoover, Phys. Rev. A **31**, 1695 (1985).
[44] L. A. Rowley, D. Nicholson, and N. G. Parsonage, J. Comput. Phys. **17**, 401 (1975).
[45] U. Essmann, L. Perera, M. L. Berkowitz, T. Darden, H. Lee, and L. G. Pedersen, J. Chem. Phys. **103**, 8577 (1995).
[46] J.-P. Ryckaert, G. Ciccotti, and H. J. C. Berendsen, J. Comput. Phys. **23**, 327 (1977).
[47] S. E. Feller, Y. Zhang, R. W. Pastor, and B. R. Brooks, J. Chem. Phys. **103**, 4613 (1995).
[48] M. Schindler, Chem. Phys. **375**, 327 (2010).
[49] I. M. de Schepper, E. G. D. Cohen, C. Bruin, J. C. van Rijs, W. Montrooij, and L. A. de Graaf, Phys. Rev. A **38**, 271 (1988).
[50] B. J. Palmer, Phys. Rev. E **49**, 359 (1994).
[51] D. Bertolini and A. Tani, Phys. Rev. E **51**, 1091 (1995).
[52] P. Schofield, Proc. Phys. Soc. **88**, 149 (1966).